ALMA MATER STUDIORUM
UNIVERSITÀ DI BOLOGNA

ARCHIVIO ISTITUZIONALE
DELLA RICERCA

Alma Mater Studiorum Università di Bologna
Archivio istituzionale della ricerca

Challenges in LICIA Cubesat trajectory design to support DART mission science

This is the final peer-reviewed author's accepted manuscript (postprint) of the following publication:

Published Version:
Challenges in LICIA Cubesat trajectory design to support DART mission science / Capannolo A.; Zanotti G.; Lavagna M.; Epifani E.M.; Dotto E.; Della Corte V.; Gai I.; Zannoni M.; Amoroso M.; Pirrotta S.. - In: ACTA ASTRONAUTICA. - ISSN 0094-5765. - ELETTRONICO. - 182:(2021), pp. 208-218. [10.1016/j.actaastro.2020.09.023]

Availability:
This version is available at: https://hdl.handle.net/11585/812800 since: 2022-10-21

Published:
DOI: http://doi.org/10.1016/j.actaastro.2020.09.023

Terms of use:

Some rights reserved. The terms and conditions for the reuse of this version of the manuscript are specified in the publishing policy. For all terms of use and more information see the publisher's website.

This item was downloaded from IRIS Università di Bologna (https://cris.unibo.it/).
When citing, please refer to the published version.

(Article begins on next page)

20 April 2024

This is the final peer-reviewed accepted manuscript of:

Capannolo, A., Zanotti, G., Lavagna, M., Epifani, E.M., Dotto, E., Della Corte, V., Gai, I., Zannoni, M., Amoroso, M., Pirrotta, S., 2021. Challenges in LICIA Cubesat trajectory design to support DART mission science. Acta Astronaut. 182, 208–218.

The final published version is available online at:

https://doi.org/10.1016/j.actaastro.2020.09.023

Rights / License:

The terms and conditions for the reuse of this version of the manuscript are specified in the publishing policy. For all terms of use and more information see the publisher's website.

This item was downloaded from IRIS Università di Bologna (https://cris.unibo.it/)

When citing, please refer to the published version.

Manuscript File Click here to view linked References

Highlights

Challenges in LICIA Cubesat Trajectory Design to Support DART Mission Science

Andrea Capannolo, Giovanni Zanotti, Michèle Lavagna, Elena Mazzotta Epifani, Elisabetta Dotto, Vincenzo Della Corte, Igor Gai, Marco Zannoni, Marilena Amoroso, Simone Pirrotta

- The LICIACube mission will serve as scientific support for NASA's DART kinetic impactor
- LICIACube will be the first CubeSat to visit an asteroid system
- Hardware limitations and the complexity of the mission narrow down the trajectory options
- Accurate optimization is adopted to identify best options for scientific return maximization
- Robustness of the selected trajectory, in presence of uncertainties and contingencies, is derived

Challenges in LICIA Cubesat Trajectory Design to Support DART Mission Science

Andrea Capannolo[a], Giovanni Zanotti[a], Michèle Lavagna[a], Elena Mazzotta Epifani[b], Elisabetta Dotto[b], Vincenzo Della Corte[b], Igor Gai[c], Marco Zannoni[c], Marilena Amoroso[d], Simone Pirrotta[d]

[a] *Politecnico di Milano*
[b] *INAF - Istituto Nazionale di Astrofisica*
[c] *Università di Bologna*
[d] *ASI - Agenzia Spaziale Italiana*

Abstract

In 2021, the DART spacecraft will be launched by NASA to intercept the binary system Didymos and impact the moonlet (Dimorphos), to test the effectiveness of kinetic impactors for the deviation of hazardous asteroids' trajectories. The impact is expected to generate a cloud of particles, whose study could provide valuable data about asteroid's properties and impact models. Observations from ground to characterize ejecta and plume evolution after impact would be possible, but the resulting quality would be significantly lower than a short-range imaging. In this framework, ASI (Italian Space Agency) and NASA started a collaboration to embark on the US DART vehicle the LICIA (Light Italian CubeSat for Imaging Asteroid) 6U CubeSat as a piggyback payload. LICIA is devoted to grasp science data by imaging the ejecta plume after the impact, and observe Dimorphos surface while flying by the binary system. The Italian consortium involved in the mission sees ARGOTEC for the platform development, and INAF, Politecnico di Milano and Università di Bologna to cover the mission science,

trajectory design and orbit de-termination tasks, respectively. The paper focuses on the mission analysis and maneuvers design, strongly driven by the science return, under the tight constraints enforced by the platform. In particular, it describes the preliminary procedure followed to derive trajectory constraints and to select the best option for the flyby. Despite the mission is still under development, and subjected to frequent updates of several parameters, the final performances derived in this paper maintain their validity as they represent the desired target values for the mission.
Keywords:
CubeSat, Deep space, Asteroid exploration, Planetary defence, Trajectory Optimization

---

1. Introduction

Asteroid and comets exploration has been a field of great interest during the past few decades (starting with the NEAR Shoemaker mission in 2001), thanks to the enormous scientific information these bodies can provide about the early formation of the Solar System. On the other hand, a large group of small bodies represents also a threat, being them very close to our planet. In such a case, an accurate knowledge would be useful to develop the best strategy for trajectory deviation techniques. The limited information available on the physical properties (shape, mass, etc.), make these bodies a high-risk environment to be explored, and to keep a safe distance is of the utmost importance. Smaller, light and low cost deployable systems can then cooperate with main spacecraft, and perform higher risk operations (e.g. Philae lander for the Rosetta mission (ESA) [1]). One of the

next targets for future missions is the binary asteroid system 65803 Didymos, which provides a unique miniature environment, perfect for testing deflection techniques through kinetic impacts. In this frame, the DART mission (NASA) will exploit a spacecraft to impact the small moon of the system, while few years later, HERA spacecraft (ESA), formerly known as AIM, will intercept the system to analyze the post-impact properties of the bodies, also through miniaturized assets [2, 3]. The delay between DART and HERA, however, is too high to observe the evolution of the impact's ejected particles, whose imaging and tracking would validate current impact theoretical models. Following the philosophy of exploiting low cost, light systems for high risk operations, this gap in the science outcome will be covered by a CubeSat, named LICIACube, that will be deployed from DART before the impact. LICIACube will be one of the first CubeSats to fly in deep space, and the absolute first to fly by an asteroid. Its main objectives are the observation of the ejected particles, and the imaging of the system, to aid the volume estimation of the impacted asteroid. The main drawback of the exploitation of a CubeSat is the reduced resources offered by the system, which poses several challenges in the mission design process. In particular, the trajectory design has to face several challenges to make the mission compliant to all the stringent constraints related to science, operations, platform, and risk. The paper carries the reader through the flow-down of such requirements and limitations into mathematical constraints for an optimization procedure that is performed as part of the baseline trajectory selection process. Section 2 introduces the mission in detail and gives a complete overview of the operational scenario. Section 3 addresses the identification of the mission

constraints that comes from the limiting factors associated with the mission. Section 4 describes the trajectory definition process, and a sensitivity analysis of the results. Section 5 defines the problems and actions to be performed as solution for two possible non-nominal scenarios. The conclusions and the roadmap for future developments are presented in Section 6.

2. Mission scenario overview

Within the planetary defence context, the DART mission will be the first test to assess the feasibility of deflecting a potentially hazardous object's trajectory through a kinetic impactor [4]. Its trajectory is designed to hit the moonlet of the binary system at high speed, Dimorphos, in late september 2020, and visibly change its kinetic energy [5].

The main objective of the 6U LICIA CubeSat is to image the binary system and the DART impact event (crater formation and ejected particles evolution). To achieve its purpose, LICIA's trajectory must ensure a sufficient period of time in proximity of the system, and maximize the amount of data gathered during this time window. LICIA will be deployed from DART before the impact, and will exploit a small cold gas thruster to deviate its trajectory and avoid the asteroid. The low thrust magnitude does not allow a capture into the asteroid system, characterized by a very low-speed natural dynamics (cm/s), therefore a flyby is the only viable option.

Considering all the requirements and constraints of the mission (that will be presented in Section 3), the set of design parameters is reduced to the release action and the maneuver execution vectors. Although analyses are carried out in the Ecliptic J2000 (or EMO2000) inertial reference frames,

the release and maneuver directions are here expressed in terms of a local inertial reference frames ("DART" reference frame), shown in Fig. 1, and built according to the following rules:

- X-axis defines the DART-Didymos relative direction
- Z-axis is perpendicular to X-axis, and lies in the plane defined by X-axis and Didymos angular momentum vector
- Y-axis completes the reference frame

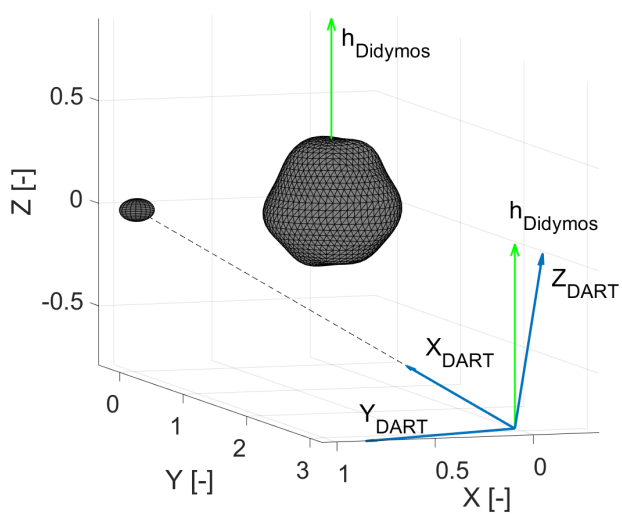

Figure 1: DART reference frame (not to scale). X axis represents the pointing direction of DART payload towards Dimorphos. Z axis is perpendiculat to X, and lies in the plane defined by X and the angular momentum vector of the binary system. Y axis completes the frame.

The two spherical angles φ and ϑ are defined in the aforementioned frame as follows:

- ϑ is the azimuth angle, defined counterclockwise from y axis in the y-z plane (range: 0° to 360°)

- φ is the elevation angle, defined from y-z plane and positive towards the -x direction (range: -90° to 90°)

Figure 2 depicts the two angles.

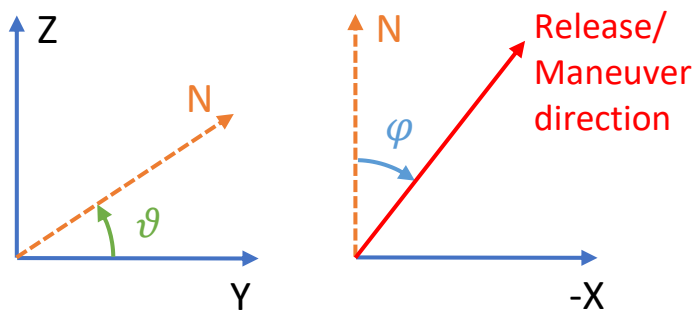

Figure 2: Spherical angles in DART reference frame.

The release ΔV is constrained in the magnitude, given by the deployment system, while the direction angles are free. The maneuver ΔV is completely free, however, previous studies showed how the best option is the full-brake maneuver (-x direction), since it allows a better control of the arrival time, leaving most of the control on the flyby distance to the release action (see [6] for details). For this reason, maneuvers angles have been fixed at $\varphi = 90°$ and $\vartheta = 0°$.

An initial high fidelity model of the environment was introduced. The main asteroid gravity was modeled according to an up-to-date polyhedral shape model [7], while the moonlet's contribution was included through a triaxial ellipsoid shape model [8]. Circular Restricted Three-Body Problem

was employed [9], with the additional perturbation effect from Solar radiation pressure. First analyses highlighted that such high fidelity model is not necessary for the design phase, due to the nature of the fly-by trajectory. Indeed, the relative velocity of the CubeSat is so high ($6.58\,\mathrm{km\,s^{-1}}$) that the actual influence of such effects is null. For such reason the trajectory selection process, which required several simulations to map all possibilities, has been performed exploiting a simplified model. The simplification consists in using a Keplerian 2-body dynamics, with a single mass for the whole binary system. After the selection of the baseline trajectory, the subsequent analyses are carried out using a full ephemeris model, considering the gravitational effect of all the Solar System planets and the Sun, plus the Didymos binary system (still modeled as a single mass). This 2-steps modeling approach allowed to speed up the computations, without affecting the accuracy of the final results.

3. Mission constraints identification

This section addresses the definition of all the constraints to be taken into account for the design of the CubeSat mission analysis. In the next subsections, each aspect will be analyzed separately, highlighting their relations with the others, to derive a comprehensive set of constraints for the final trajectory baseline selection.

3.1. Scientific objectives

The objectives that the CubeSat has to fulfill in terms of science are driven by the nature of its mission, i.e. to provide documentation of the

DART impact, by acquiring visual data of the immediate post-impact scenario. Particular attention is posed on the imaging of the impact surface, in order to extract data on the formed crater and on the generated ejecta plume. The collection of images will help the characterization of crater formation and of the impact process, and will provide useful information about the dynamics of ejected particles. Moreover, another observation target is related to the non-impacted hemisphere of Dimorphos, i.e. the side not visible from DART point of view, in order to reconstruct the shape of the body. These objectives are formalized as scientific requirements as follows [10].

- Obtain at least three images of the DART impact site, in order to measure the size and morphology of the impact crater. Sufficient delay time, from DART impact to CubeSat close approach, shall be achieved, so that neighborhood of the crater is cleared from the particles cloud. The image resolution shall be better than 1 m/px.

- Obtain at least three images of the ejecta plume at different times and phase angles, in order to measure the motion of slow ejecta (i.e. slower than $5\,\mathrm{m\,s^{-1}}$) and to allow the estimation of the density structure. The slow particles shall be observed over a time-span of at least 30 s, with an image resolution better than 5 m/px.

- Obtain images of the ejecta plume and of the target asteroid to characterize both color and spectral variations during the fly-by.

- Obtain at least three images of the non-impacted hemisphere, in order to better reconstruct the body volume and shape model. The required resolution shall be better than 2 m/px.

The objectives list defines many constraints for the mission analysis, either in terms of trajectory and of operations. In particular, resolution and delay time affect the flyby distance and the Δv cost of the maneuvers respectively. Their effect will be presented in the next subsection, in relation to the other constraints.

3.2. Ejecta

Crater and Ejecta formation models.. In order to completely characterize the environment the CubeSat will be exposed to during the fly-by, the presence of ejecta generated during the DART impact requires a proper modelization. The complete impact event can be subdivided into two different phases, i.e. a *fragmentation* and a *re-accumulation*. The first step consists in the collision between the two objects that generates the displacement of a huge amount of material, leading to the crater formation and the ejecta generation. During the second phase, the newborn fragments evolve in the dynamical environment of the binary system and eventually collide with one of the two asteroids, escape the gravitational influence of the system or remain in a bounded region in its neighborhood. The characteristic timescales of the two phases differ by orders of magnitude, justifying the choice of simulating them separately. If the gravitational re-accumulation phase can be managed only by direct integration of the proper equations of motion for each of the generated fragments, to properly model the fragmentation phase, different approaches can be exploited, either analytical or numerical. The so-called *scaling laws* proposed and developed by Holsapple and Schmidt in [11] are the most suitable among the analytical methods: simple correlations between the input parameters of the impactor-target couple and the bulk outputs of

the event are defined. These correlations are obtained by exploiting dimensional analysis and some logical assumption, before fitting a great quantity of experimental data, from different lab-scale experiences in hyper-velocity impacts. Among the outputs there are, e.g., volume and radius of the formed crater and initial velocity of each ejectum, as function of its radial distance from the impact point. A detailed review and summary of all the scaling laws are found in [12]. Different schemes have been implemented to deal with the impact obliquity, particle size distributions and ejecta sampling, as described in [13, 14, 15, 16]. Collecting all these contributions, it is possible to generate the ejected particles, randomly placed along the radial distance up to the radius of the crater and to associate a related velocity, leading to a complete state vector for each item. [12] quantifies non-physiscal constants for the scaling laws, according to different target compositions. The three materials which may be actually plausible to consider for the unknown asteroid composition are reported in Table 1. Figure 3 shows the plume geometry

Table 1: Asteroid possible compositions with different porosity values. Bas = Monolithic Basalt, WCB = Weakly Cemented Basalt, SFA = Sand/Fly Ash. Values taken from [12].

	Bas	WCB	SFA
Density [kg/m^3]	3000	2600	1500
Porosity	0%	20%	45%
Strength [MPa]	30	0.45	0.004

got by applying the scaling lasw modelling approach, according to the three selected asteroid possible compositions. The basaltic composition has been

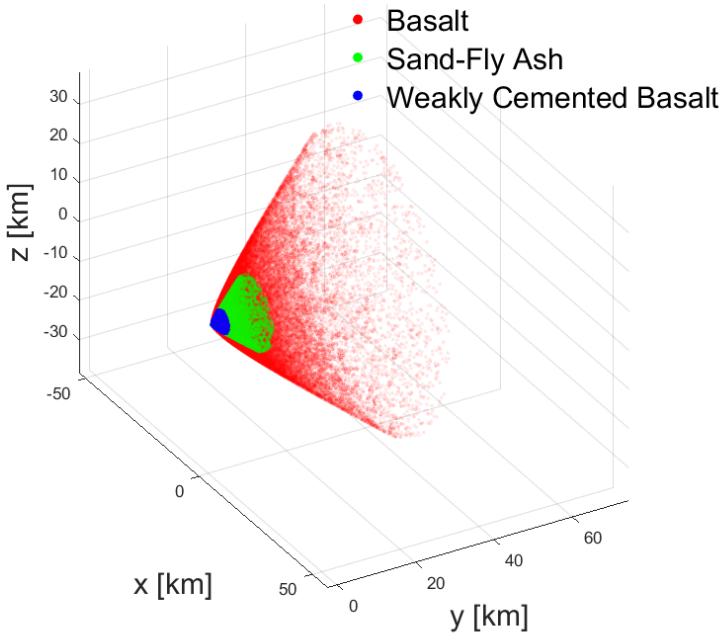

Figure 3: Ejecta plume geometry with the three different compositions overlapped, Basalt in red, WCB in blue and SFA in green, taken 260 s after DART impact. The origin of the coordinate frame coincides with the impact point on Dimorphos, which at this scale is imperceptible.

taken as reference case since the associated plume is the most expanded. Such condition represents a worst case scenario for LICIACube safety concerns.

If the numerical method is pursued, various classes of solvers can be chosen to deal with the fragmentation simulation, but in a hypervelocity impact scenarios, the extreme deformations induced to the material suggest to prefer a meshless over a grid-based method. Among the meshless methods, the *Smoothed Particle Hydrodynamics* (SPH) method, with its deep utilization both in astrophysics and fluid dynamics fields makes it the most mature. In addition, it has shown promising results also in the field of hypervelocity impacts. In the context of this work, the SPH simulations performed with the commercial code *LS-Dyna*®have presented similar results to those obtained with the scaling laws, assuming the characteristics of monolithic basalt in both methods. The details of the implementations can be found in [17] and [18]. Figures 4 and 5 show the comparison between the two methods, in terms of crater size, shape, density and ejecta velocity.

There is a fair agreement in the size of the crater, the ejection velocity magnitude and the ejection angles, while the crater shape and the ejecta layer thickness differ slightly. Given the agreement found among the two approaches, the choice of continuing with the *scaling laws* method has been taken, since it performs much better in terms of simplicity and computational burden. Moreover its versatility in terms of generating stochastic formulations can be perfectly exploited for sensitivity studies in support of the mission analysis.

Sensitivity Studies. To perform the fly-by, broadly speaking, two main alternatives can be taken in consideration: passing through the plume cone

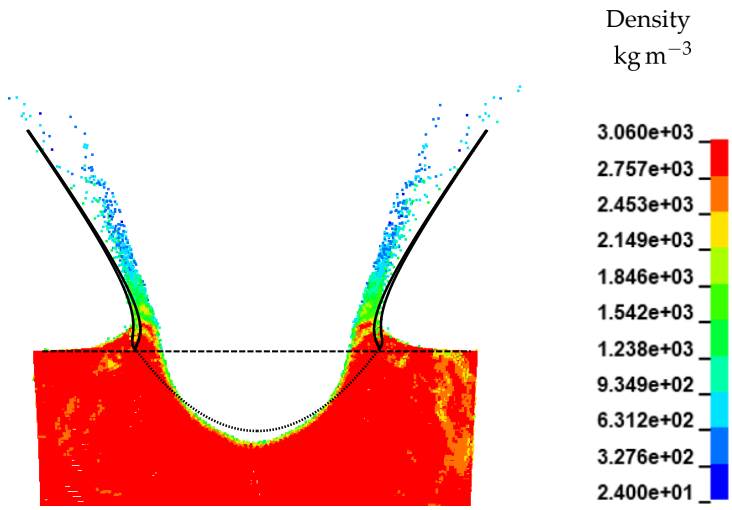

Figure 4: Comparison of crater's section in the analytical (black lines) and numerical (with density color code) methods at 60ms after the impact.

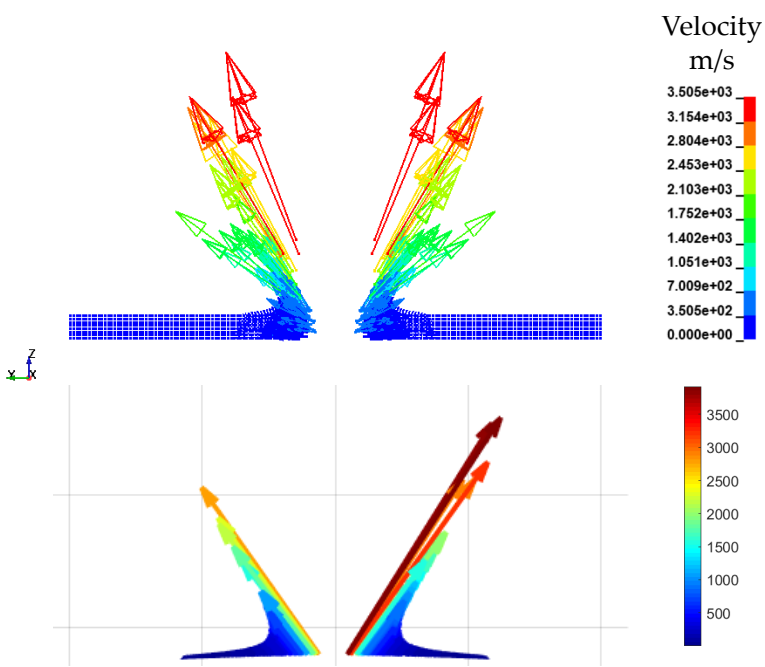

Figure 5: Comparison of the ejection velocity vectors with SPH (up) and scaling laws (down).

or avoiding it. The idea behind the first strategy is that of pushing at the minimum the close approach distance to the asteroid, in order to get the best resolution on the crater imaging. Even if appealing, such option, in order to be viable, must comply with safety concerns. Indeed the possibility for the CubeSat to be hit by an ejectum has to be taken into account and studied. To assess such a risk, a simple model to estimate the penetration of an ejectum into the CubeSat panels or optics has been used, as proposed in [19]. Assuming a relative velocity between CubeSat and ejectum of $6\,\mathrm{km\,s^{-1}}$, a minimum threshold of ejecta diameter has been identified as the smallest dangerous particle. This value has been set to 0.1 mm, as a size able to penetrate up to around 20% of the thickness of the cited components. Thus, a Monte-Carlo analysis has been performed by randomly generating 500 different ejecta clouds with diameters in the range $0.1\,\mathrm{mm} \div 10\,\mathrm{cm}$ and then estimating the probability of encountering at least one fragments at different distances from Dimorphos, assuming an effective exposed surface area of $1\,\mathrm{m}^2$ for the CubeSat. The results reported that the probability of encounter stays fixed at 100% up to a maximum distance from Dimorphos where it steeply falls down to 0%. This fall reflects the high difference in particle space concentration due to a sharp outer edge of the ejecta plume. The value of such maximum distance depends on the time after the impact and with a delay time of 260 s it stays near 20 km. Such outcomes highlight the unfeasibility of the first strategy and the need of ensuring, considering all the associated uncertainties, the actual trajectory of the CubeSat not to pass below this boundary distance by setting a proper constraint. Such constraint was defined as keeping the CubeSat always at least 15 km away from

the plume outermost ejecta. Consequently, a *dummy* particle has been generated and taken as outermost ejectum of the plume, lying on the plane defined by the Cubesat trajectory and Dimorphos. Such particle is initialized with the maximum ejection velocity and the minimum ejection angle (i.e. wider cone aperture), corresponding to a fake condition, following the scaling laws model. Indeed, the maximum ejection velocity magnitude is associated to the particles ejected from the inner part of the cone. Such approach can guarantee a certain robustness in the proposed trajectory, considering also the fact that both the actual composition of the asteroid and conformation of the impacted surface will remain unknown.

3.3. DART & Didymos

The DART spacecraft's state presents variable level of uncertainty for the whole duration of the mission, with a steep drop in the last days before impact, thanks to visual target acquisition [20]. Similarly, current ephemeris of Didymos system is subjected to a certain level of inaccuracy, which will decrease as DART will approach the binary system.

A late release of the CubeSat would provide a minimized uncertainty, however, it would not offer enough time for a proper separation and observation of the impact and ejecta (as explained in Section 3.1). Furthermore, the time for backup maneuvers and contingency operations would be too short (see Section 5). Consequently it is necessary for the CubeSat to be released earlier than the last few hours. In waterfall, the higher DART uncertainties at release (as depicted in Fig. 6) shall be considered, as they play an important role.

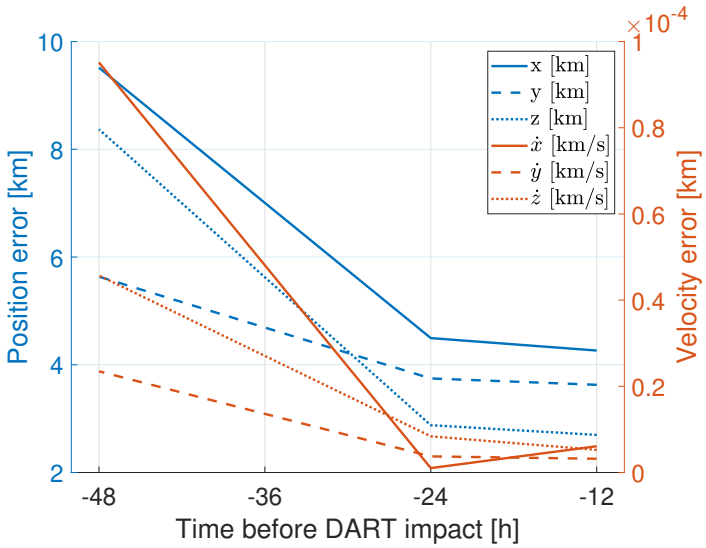

Figure 6: DART state uncertainty evolution with time

Table 2 reports the state determination errors for DART up to 48 hours prior to impact, while for earlier times the uncertainty is assumed to be constant and equal to the $T_0 - 48h$ value.

3.4. CubeSat Hardware

The Cubesat components represent one of the main sources of disturbance for the correct execution of the flyby, given the typical reduced performances of nanosatellites. The analyses identified four main components as the most constraining sources for the trajectory design:

- Dispenser
- Thruster
- Camera
- ADCS

States	$T_0 - 12h$	$T_0 - 24h$	$T_0 - 48h$
x $[km]$	4.264	4.495	9.515
y $[km]$	3.628	3.746	5.636
z $[km]$	2.698	2.878	8.371
$\dot{x}$ $[km/s]$	6.095×10^{-6}	1.023×10^{-6}	9.515×10^{-5}
$\dot{y}$ $[km/s]$	3.191×10^{-6}	3.736×10^{-6}	2.348×10^{-5}
$\dot{z}$ $[km/s]$	5.249×10^{-6}	8.397×10^{-6}	4.572×10^{-5}

Table 2: DART-Didymos relative state uncertainty with respect to time before impact (T_0), in EME2000 reference frame

Dispenser. The dispenser is a 6U container provided with rails an redundant springs for the deployment. It is mounted on a DART lateral panel. It has been designed with an inclination of 10° away from solar panels direction, such that the chances of hitting them is minimized.

The main sources of uncertainty from the dispenser are related to the spring pushing force, and the dynamics of the CubeSat at the dispenser's rails end. Furthermore, a non-negligible effect may be given by the reaction torque that the CubeSat gives to DART spacecraft, which can relevantly change the release direction.

Considering the aforementioned effects, the following uncertainties have been selected for the release maneuver:

- $\sigma_{\Delta v_{rel}} = 0.07\ m/s$
- $\sigma_{\varphi_{rel}} = 2\ ^\circ$
- $\sigma_{\vartheta_{rel}} = 2\ ^\circ$

Thruster & ADCS. With the thrusters and the ADCS systems still being in a design refinement process, the disturbances related to them have been defined according to expected values, and will be refined once the precise design of these systems will be frozen.

The baseline model adopted for the thruster is the ArgoMoon propulsion system, which can provide 100 mN of thrust and an overall Δv of 56 m/s for a 14 kg CubeSat. However, to reduce weight, a lower performance system is being evaluated by ArgoTec: currently, a thrust of 50 mN is being considered. The uncertainty adopted for the thruster is related to the burn time, and it is set to 3 seconds.

The ADCS system is in a design refinement phase as well, and therefore its uncertainties has been defined through an educated guess, which will be refined later. In particular, the output from ADCS performances are the two spherical angles defining the thrust direction, namely φ_{burn} and ϑ_{burn}. The 1-sigma value is assumed to be 1.1°for both.

Wrapping up the uncertainties related to the maneuver action, the 1-sigma values are:

- $\sigma_{t_{burn}} = 3\ s$
- $\sigma_{\varphi_{burn}} = 1.1\ ^\circ$
- $\sigma_{\vartheta_{burn}} = 1.1\ ^\circ$

Camera & Reaction wheels. The CubeSat camera and the ADCS actuators (namely the reaction wheels) are the most affecting hardware for the mission design, and their constraints are strongly related to each other, hence the two components shall be considered together.

While LICIA will mount two cameras, a narrow angle (NAC) and a wide angle (WAC) one, the most stringent constraints are given by the NAC camera, which will be operating during the whole flyby, and will provide images of the plume and, possibly, the crater. The NAC camera has a diagonal FoV of $\pm 2.05°$, an IFOV of $25\mu rad$, and a sensor dimension of 2048x2048 pixels. The three scientific objectives have resolution thresholds of 1 m/px, 2 m/px and 5 m/px. Considering the camera properties, this translates in a maximum flyby distance of 40 km, 80 km and 200 km respectively.

As a second constraint provided by the camera, to properly image the ejecta after the impact, it it necessary to have a dark background, avoiding a visual alignment with the primary asteroid. This implies that the flyby trajectory shall be out-of-plane with respect to the binary system orbital plane. This also benefits the imaging condition, avoiding large variations in the Sun aspect angle (as shown in Section 4), and, consequently, providing a better condition for achieving a high quality imaging of the plume.

The reaction wheels performances are designed to allow a constant pointing of the moonlet of the system during the whole flyby. However, an excessively close flyby distance would inevitably cause a saturation of the wheels, thus making the CubeSat loose the target. In particular, the current design of the wheels allows a maximum rotation rate of the CubeSat of 8.57 deg/s, and a maximum angular acceleration of 1.2 deg/s^2. The angular rate revealed to be the most constraining parameter, preventing the flyby distance from being reduced below 44 km. As a consequence, the current design of the platform does not allow to observe the crater at a proper resolution (at least 1 m/px), therefore a resolution of 2 m/px, corresponding to a distance of 80 km, is fixed

as new maximum resolution to be achieved by the spacecraft. The resulting nominal flyby distance shall be such that $44km \leq d_{CA} \leq 80km$; however, a margin of at least 3 km is taken into account, given the uncertainties in release and maneuvers operations, plus the uncertainty of the DART-Didymos relative position and velocity. It is noted that the constant target pointing strategy, despite feasible in terms of reaction wheels saturation limits, may introduce some issues related to the attitude control and, consequently, to the quality of the observations (e.g. blurred images). Although not addressed in this paper, it is acknowledged the necessity of a proper design for the attitude controller and a thorough analysis of its response, coupled to the evaluation of achievable images quality.

3.5. Mission Operations

Operations put tight constraint in the selection of the final trajectory. To avoid any interference with DART operations during the final approach and impact phases, the CubeSat must be relased as soon as possible. However, from Section 3.3, it is acknowledged the large increase in DART uncertainty related to excessively soon releases. The trade-off proposed in this paper is a release 5 days before impact, which provides several hours left for possible contingency scenarios (presented in Section 5).

Considering the uncertainty presented in previous subsections, a 5 days trajectory propagation would cause the deviations to grow enough to make the deviation unacceptable. A correction maneuver is therefore designed 1 day before DART impact, based on updated navigation parameter through frequent DSN contacts during the preceding 3 days. Details on deviations and correction maneuver are presented in Section 4

4. Baseline scenario analysis

4.1. Nominal trajectory design

The selection of the baseline followed a preliminary mapping of the search space, satisfying all the constraints described in the previous section, by computing a set of trajectories as function of release angles φ and ϑ. In particular, fixing the release angles, and imposing the maneuver direction angles to $\varphi_{burn} = 90°$ and $\vartheta_{burn} = 0°$, the trajectory is computed according to the problem 1:

$$\begin{aligned} \max_{\Delta t_{burn}} \quad & t_{delay} \\ \text{subject to} \quad & 0 \leq \Delta t_{burn} \leq \max(\Delta t_{burn}), \\ & \Delta T_{5\,\mathrm{m/px}} > 30\,\mathrm{s}, \\ & d_{Ejecta} > 15\,\mathrm{km}, \\ & 44\,\mathrm{km} \leq d_{C/A} \leq 80\,\mathrm{km}. \end{aligned} \tag{1}$$

where Δt_{burn} is the time interval of the maneuver execution, t_{delay} the time from DART impact to LICIA close approach, $\Delta T_{5\,\mathrm{m/px}}$ the time interval at which a resolution below 5 m/px is achieved, d_{Ejecta} the minimum distance from the expanding ejecta cone reached by the CubeSat, and $d_{C/A}$ the distance from the binary system's moonlet at close approach. The solutions of problem 1 allow defining all feasible trajectories, whose arrival time to the system is the latest possible, with the purpose of maximizing the expansion of the ejecta and facilitate the visibility of the crater. Notice that, due to the maximized cone expansion, the minimum distance from ejecta of the optimized solution is always close to the lower boundary of the corresponding constraint.

Each trajectory is evaluated in terms of a single, scalar, score, defined as a summation of sub-objectives to be fulfilled, i.e.:

- Enhance resolution (Minimize close approach distance)
- Improve crater's visibility (Maximize delay time)
- Increase science time (Maximize time interval at resolution 5 m/px or better)
- Reduce reaction wheels load from target pointing (Maximize close approach distance)

The corresponding cost equation is defined as follows:

$$J = \frac{J_{res} + J_{vis} + J_{sci} + J_{rw}}{4} \tag{2}$$

with

$$J_{res} = \frac{res - \max(\mathbf{res})}{\min(\mathbf{res}) - \max(\mathbf{res})} \tag{3}$$

$$J_{vis} = \frac{t_{delay} - \max(\mathbf{t}_{delay})}{\min(\mathbf{t}_{delay}) - \max(\mathbf{t}_{delay})} \tag{4}$$

$$J_{sci} = \frac{\Delta T_{5\,\mathrm{m/px}} - \max(\mathbf{\Delta T}_{5\,\mathrm{m/px}})}{\min(\mathbf{\Delta T}_{5\,\mathrm{m/px}}) - \max(\mathbf{\Delta T}_{5\,\mathrm{m/px}})} \tag{5}$$

$$J_{rw} = \frac{\omega_{peak} - \min(\boldsymbol{\omega}_{peak})}{\max(\boldsymbol{\omega}_{peak}) - \min(\boldsymbol{\omega}_{peak})} \tag{6}$$

being the bold characters referred to full parameter set from all the generated trajectories. Cost terms 3 and 5 are minimized at closer flyby distance (a reduced distance allows to achieve a better resolution, and a longer time of observations above minimum resolution threshold), while terms 4 and 6 reach their smallest values at farther close approach distances (slower CubeSat

spin for target pointing, and longer time for ejecta cone expansion allowed). The two couples of conflicting objectives generate a convex shape of the overall cost defined in 2, as shown in Fig. 7. It is here underlined that the

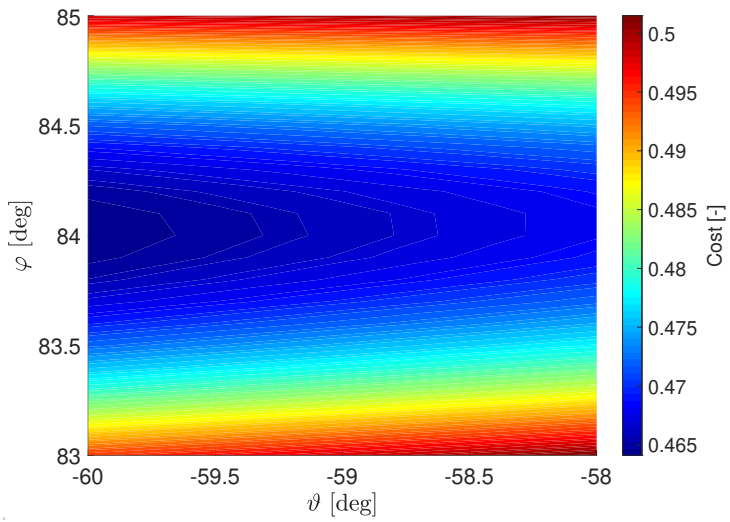

Figure 7: Map of the overall cost, as a function of the release angles. φ is bounded by the close approach distance constraints. ϑ lower bound is enforced to avoid large Sun aspect angles, while the upper bound has been set to equally scale the two axes.

greater curvature is measured along the axis defining the φ variation, whereas mild, monotonic reduction of the cost is present along the ϑ axis, with the minimum located in the most negative values region. Despite the monotonic reduction along ϑ direction, a minimum threshold of $-60°$ is enforced, to avoid excessively large sun aspect angles, detrimental to the observations (being the Sun approximately on the equator plane of the asteroids). A global minimum is then found at $\varphi = 84°$ and $\vartheta = -60°$, and the corresponding trajectory parameters are reported in Table 3.

φ_{rel} [deg]	Δv [m/s]	t_{delay} [s]	$d_{C/A}$ [km]	Max Res [m/px]	ω_{max} [deg/s]	$\Delta T_{5\,\mathrm{m/px}}$ [s]
84	2.1	209.4	55.2	1.38	6.823	58.4

Table 3: Cost optimal trajectory parameters

The low cost region depicted in Fig. 7 was then explored to search for nearby trajectories which could enhance science while respecting platform limitations, justified by the mild variation in the cost function. It was proposed a second option (named "enhanced science", as opposed to the previous "cost optimal" solution), close to the high φ region of the map, which would enhance the resolution of the observation, as shown in Table 4. It can be

φ_{rel} [deg]	Δv [m/s]	t_{delay} [s]	$d_{C/A}$ [km]	Max Res [m/px]	ω_{max} [deg/s]	$\Delta T_{5\,\mathrm{m/px}}$ [s]
84.9	1.43	167.1	47	1.18	8.018	59.1

Table 4: Enhanced science trajectory parameters

noticed that the relatively small improvement in resolution and observation time below 5 m/px is associated with a large reduction of the delay time and a significant increase in the peak spin of the satellite, which approaches the saturation limit. A Monte-Carlo analysis was performed, considering the errors and uncertainties listed in Section 3, highlighting a frequent occurence of reaction wheels saturation for the enhanced science option. In particular, saturation was observed around 23 % of cases, against the 0.1 % of the cost optimal solution. The spin peak distributions are depicted in Fig. 8a.

While the saturation problem can be solved through a preload of the reaction wheels, it was also observed that the already poor improvement in the nominal resolution of the observations is overshadowed by the large probability distribution from the Monte-Carlo analysis. Figure 8b shows how a large portion of the two distributions is overlapped, and similar quality of images from both trajectories are to be expected.

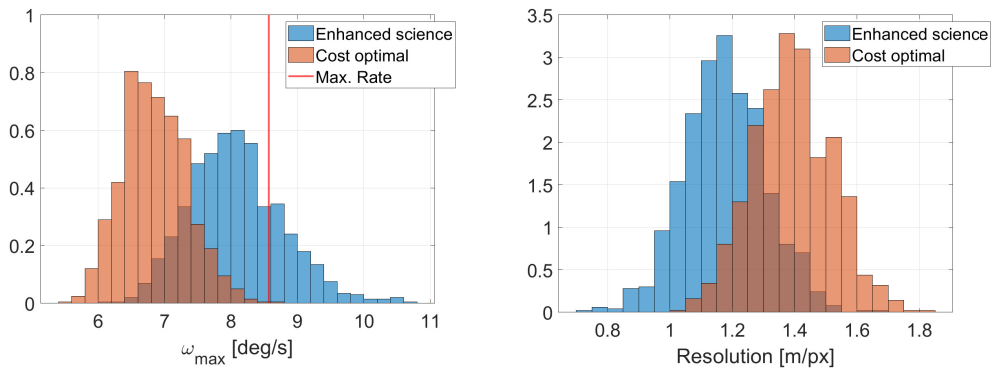

(a) Max spin rate distributions. Red line represents the limit value from reaction wheels saturation.

(b) Max resolution distributions

Figure 8: Max rate and resolution distributions comparison between the enhanced science and the cost optimal trajectories.

According to the aforementioned findings, the cost optimal trajectory was selected as basis for the baseline definition. Nevertheless, subsequent science analyses highlighted how the delay time of 209.4 s could undermine the scientific objective of plume observation. In fact, such time interval would cause the ejecta cone to expand too much, drastically reducing its density and hindering its detectability by the camera sensor. Furthermore, a study on crater visibility and size on the sensor showed that, regardless of the expansion level of the ejecta, the relative diameter in pixels, projected on

sensor surface, is extremely small even for the enhanced science trajectory, as depicted in Fig. 9.

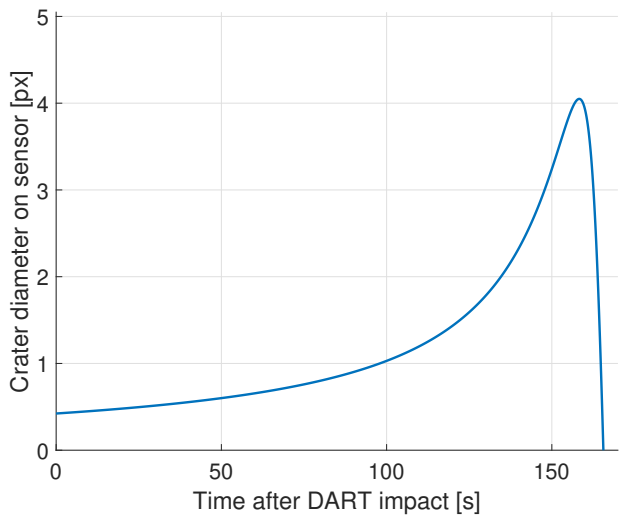

Figure 9: Equivalent crater diameter in pixels, as observed by the sensor during close approach (enhanced science trajectory). The crater is assumed to have a diameter of 12.2 m, coherently to the best case among assumed materials for the asteroid.

Viceversa, the delay time measured for the enhanced science option revealed to be optimal for observation. For this reason, a baseline trajectory is built starting from parameters of the cost optimal option, and corrected to approximate the delay time value of the enhanced science option. The full set of the baseline's parameters is reported in Table 5. Notice that the release angle φ differs from the cost optimal trajectory of one tenth of degree, due to the slight coupling between the maneuver direction and magnitude, and the close approach distance. Also, the delay time reduction causes, as beneficial side effect, a higher distance from ejecta, thus making the trajectory safer. The angle ϑ, instead, is kept constant at the lower threshold of $-60°$, as it

$\varphi_{rel}/\vartheta_{rel}$ [deg]	Δv [m/s]	t_{delay}	$d_{C/A}$	Max Res	ω_{max}	$\Delta T_{5\,\mathrm{m/px}}$
83.9/-60	1.43	167	55.2	1.38	6.823	58.4

Table 5: Selected baseline parameters

displayed also a good trend for the Sun aspect angle, which remains bounded between 50° and 60° approximately, until the close approach (as depicted in Fig. 10).

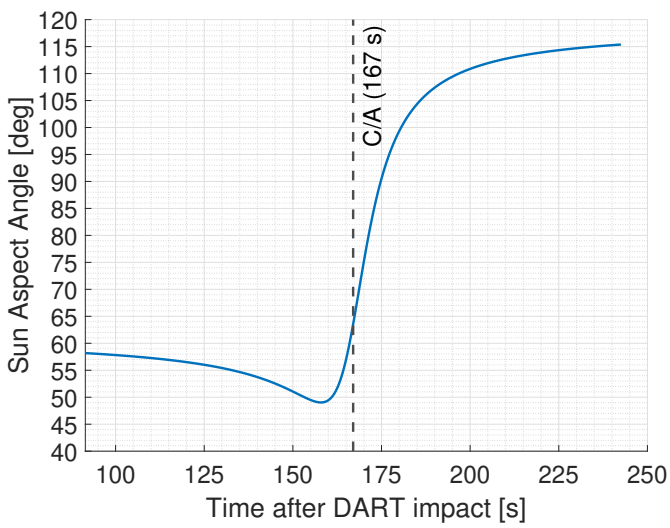

Figure 10: Sun aspect angle evolution for the selected baseline. The vertical dashed line represents the instant of the nominal close approach.

The performance related to the time windows for observations are useful for the selection of the trajectory, however, they do not represent the actual time available for the various observations required by the mission. In fact, the plume observation will be possible only around the first half of the pas-

sage, while the backside observation will occur in the second half. In practice, the time windows for each observation type are not evenly distributed, due to the inclination of DART and LICIA trajectories and the different resolution requirements. The actual time spans for the science objectives are identified by the events described in Table 6. This paper refers to Dimorphos hemispheres as the two halves of the moonlet divided by the "x-z" plane, being "x" the direction of alignment of the two asteroids, and "z" the angular momentum direction of moonlet's orbit around the primary. Also, the "back side" of the moonlet is referred to as the portion of the asteroid opposite to impact site and delimited by the visibility boundary from DART spacecraft (or back side terminator).

Science Objective	Start Event	End Event
Ejecta observation	Reach 300 km distance (5 m/px)	Dimorphos hemisphere crossing
Back side observation	Back side terminator crossing	Reach 80 km distance (2 m/px)

Table 6: Observation time events definition

Note that, due to the slight difference between hemisphere and back side definitions, there will be a short transition time interval in which the ejecta observation has ended, but the back side observation has not started yet. Nevertheless, part of the plume will allegedly still be visible, and part of the back side would be in sight too. Therefore, the value presented in this paper are to be considered as lower boundaries, and a slight increase in both the observations times should be expected. For a future refinement of

the performances of the trajectory, it should be also noticed that the close approach (and the best resolution achieved by the camera) is reached while being in this transition time window. The values for available observation times are reported in Table 7, where the total observation time includes also the transition time.

Ejecta	Back side	Transition	Total
27.2 s	8.1 s	2.7 s	38 s

Table 7: Availbale observation time widows for the scientific objectives

4.2. Robustness analysis

A detailed robustness analysis has been carried out through a Monte-Carlo analysis, based on the nominal parameters of the baseline, and considering all the uncertainties listed and described in Section 3. Each set of perturbed parameters is propagated for the whole expected duration of the mission, and main performances variation has been recorded.

A first scenario, without orbit determination and correction maneuvers, was considered, to assess the impact of the uncertainties values on the mission. The results showed a severe impact on the close approach, with an uncertainty cloud larger than the nominal flyby distance, as depicted in Fig. 11. The close approach location, and all distance-related events (such as reaction wheels saturation, or the maximum achievable camera resolution), become unpredictable, thus making the scenario infeasible. Furthermore, the delay time is subjected to wide variations, with a degradation of the plume observations (see Fig. 12). In the second scenario, a continuous tracking of

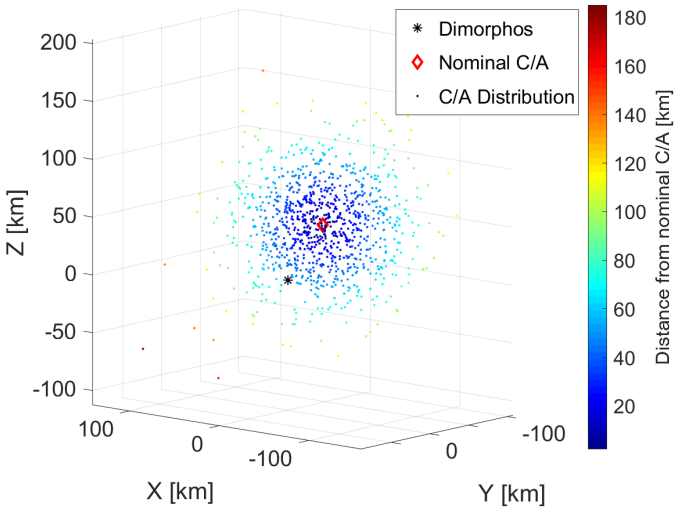

Figure 11: Close approach location cloud in EMO2000 reference frame. View aligned with the direction of spacecraft's velocity relative to the asteroid, at close approach.

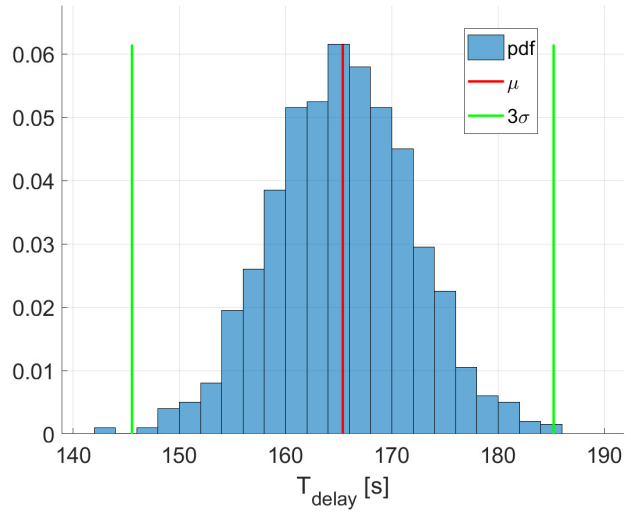

Figure 12: Delay time uncertainty (scenario without correction maneuvers)

the CubeSat is assumed, exploiting Deep Space Network (DSN) range and doppler measurements. The execution time for the correction maneuver has been selected from a trade-off considering:

- Orbit Determination accuracy: increases with time, thanks to the longer tracking time from ground stations (late maneuver)
- Contingency scenarios: a time window, prior to flyby, is required to allow additional maneuvers in case of failures and/or non-nominal events (early maneuver)

As a result, the maneuver has been placed one day before DART impact. In this way the CubeSat can be tracked for 4 days, and 1 day is left for possible contingency operations and maneuvers. The correction ΔV vector is computed through a simplified analytical model, here described. The spacecraft perturbed trajectory and the reference trajectory are approximated as straight lines from the correction maneuver location to the close approach. The maneuver direction is set to be aligned to the local position error (the difference between perturbed and reference states) at the time of the maneuver. The magnitude of the maneuver is computed through the burn time, imposing a null position error at the close approach instant. Velocity error at close approach is ignored; however, the smaller errors on velocity make this approach effective. In case of an impulsive maneuver, the correction ΔV would be equal to:

$$\|\Delta V_{corr}\| = \left\| \frac{\Delta X_{err}}{\Delta t_{C/A}} + \Delta V_{err} \right\| \tag{7}$$

with ΔX_{err} and ΔV_{err} being the deviation of position and velocity from the reference trajectory, respectively, and $\Delta t_{C/A}$ the time interval from the

correction maneuver to the nominal close approach time. Since a low thrust maneuver is considered, the correction trajectory first follows a quadratic curve (while a constant acceleration is provided by the thruster), then a linear coasting branch, in which the CubeSat's free motion aims at the reference close approach point. Given the new described geometry of the correction procedure, the burn time is defined from the solution of a quadratic equation, and reads:

$$\Delta t_{burn} = \Delta t_{C/A} - \sqrt{\Delta t_{C/A}^2 - 2\frac{M}{T}\|\Delta X_{err} + \Delta V_{err} \cdot \Delta t_{C/A}\|} \tag{8}$$

where M and T are the spacecraft mass and engine thrust respectively, and a null mass variation (negligible fuel consumption) is assumed for the maneuver. The corresponding correction cost reads:

$$\|\Delta V_{corr}\| = \frac{T}{M} \cdot \Delta t_{burn} \tag{9}$$

The robustness analysis showed that the ΔV required for correction is comparable to that of the first ("braking") maneuver. It has a mean value of 0.76 m/s and never exceeds 2 m/s (Fig. 13 shows its distribution).

Table 8 summarizes the performance variations of the trajectory, in terms of mean value and 1 sigma deviations:

Δv_{corr} [m/s]	t_{delay} [s]	$d_{C/A}$ [km]	Max Res [m/px]	ω_{max} [deg/s]	$\Delta T_{5\,\mathrm{m/px}}$ [s]
0.76 ± 0.32	167 ± 0.7	55.2 ± 5.3	1.38 ± 0.13	6.823 ± 0.472	58.4 ± 0.4

Table 8: Uncertainty distribution of main trajectory performance

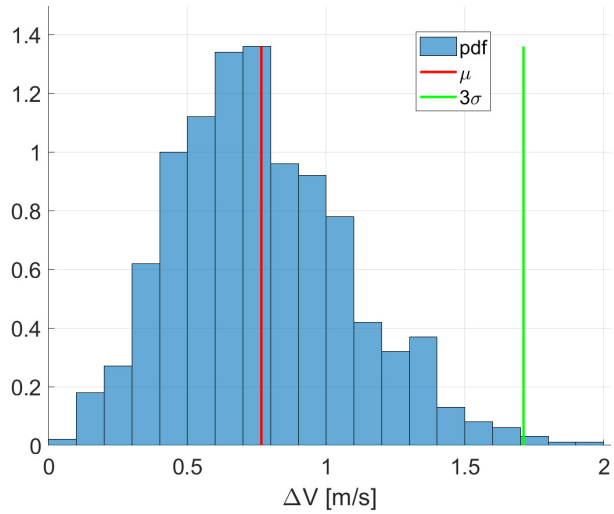

Figure 13: Correction maneuver probability distribution

5. Contingency scenarios

The baseline trajectory has been analyzed also in presence of non-nominal events, to assess the impact of failures on the mission success, and the required changes in the trajectory to restore the original performances. Two main scenarios have been selected for the analysis:

- Delayed release: failure of the nominal release action, and delayed release of the CubeSat.
- Delayed maneuver: failure of the CubeSat engine, and delayed thrusters ignition

Each scenario is analyzed and its effects on the trajectory discussed.

5.1. Delayed release

If a failure in nominal release occurs, the new window to deploy the CubeSat will be driven by DART spacecraft operations. In particular, a second and last opportunity is available 72 hours before impact. The parameters available for the tuning of the contingency scenario are the release direction and the first maneuver ΔV. Although the maneuver direction could be tuned as well, results showed that a fixed direction gives satisfactory results, while adding an attitude maneuver would represent an additional source of uncertainties.

The first analysis for the delayed release scenario is devoted to the assessment of the trajectory performances degradation, if no change on the baseline parameters is introduced. The outcome of this study demonstrates that an update on the parameters is required. In fact, the lower time available after deployment causes a strong reduction in the final close approach distance and delay time, leading to the saturation of reaction wheels, and to a less expanded ejecta cone. To restore the baseline performance, the burning time of the thruster has been increased from 400 seconds to 907 seconds, leading to a ΔV of 3.24 m/s. The release angle φ_{rel} has been decreased from 83.9°to 79.3°. It is observed how the requested effort, in case of a delayed release, is still far below the CubeSat's engine capabilities, despite the doubled magnitude of the braking maneuver.

Table 9 shows the comparison between performances for the delayed release trajectory, with constant and updated parameters.

Parameters	Baseline	Adapted
$\varphi_{release}[deg]$	83.9	79.3
$t_{burn}[s]$	400	907
$\Delta v[m/s]$	1.43	3.24
$t_{delay}[s]$	98.2	165.4
$d_{C/A}[km]$	32.7	55.3

Table 9: Main performances comparison between late release options (baseline parameters and adapted parameters)

5.2. Delayed maneuver

If the engines that are on board fail in providing the thrust action at the right time, the operation has to be rescheduled. In the context of such possibility, a sensitivity analysis on the effects of a delayed maneuver on the fly-by characteristics has been performed.

The main parameter of interest for such analysis is the maneuver epoch, computed as the time (in hours) after the release, ranging from the nominal value, i.e. 3.5 h, up to a maximum of 95 h. Three different strategies have been considered as possibilities impacting the operations of the CubeSat:

A) Keep the maneuver unchanged in both magnitude and direction.

B) Change maneuver's magnitude only.

C) Change maneuver's magnitude and direction.

The attention of such analysis is put on the flyby performances, and particularly on the effects on the delay time and the close approach distance, as seen in Fig. 14.

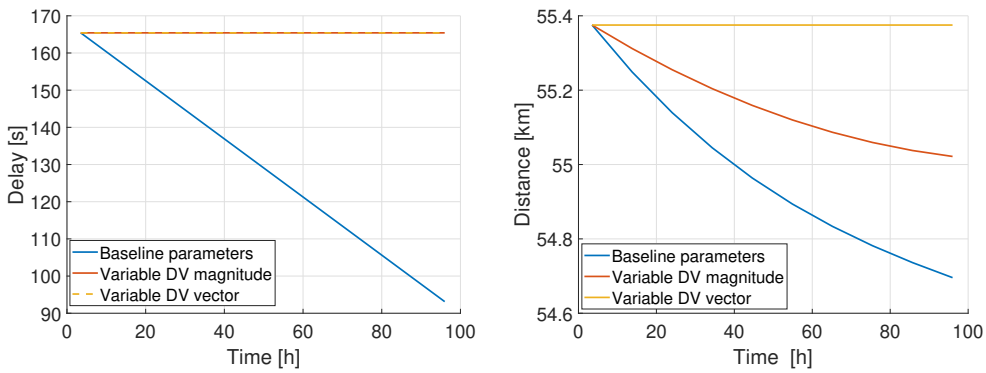

(a) Delay time

(b) Close approach distance

Figure 14: Delay time and close approach distance as function of the maneuver delay, with fixed maneuver parameters (blue line), variable magnitude (red line), and variable magnitude and direction (yellow line).

If the maneuver is kept unchanged with respect to the nominal case (blue lines) both the delay time and the close approach distance decrease. In particular, the former drastically drops by several tens of seconds, possibly jeopardizing the fly-by strategy, while the change of the latter remains confined in less than 1 km. The correction of the maneuver's magnitude alone is able to recover the nominal delay time, but not the close approach distance. In order to recover also this latter quantity, the maneuver's direction has to be corrected accordingly. Nevertheless, the only-magnitude tuning shows very small variations in the close approach distance, and represents a simpler option in terms of operations, hence this alternative has been selected as back-up strategy. The highest value of the ΔV becomes $\sim 7\,\mathrm{m\,s^{-1}}$, which is a reasonable value compared to the ΔV budget of the CubeSat. The correct epoch of maneuver execution has to be then decided by operational con-

straint, that may also be connected to the detection of the fault that caused the maneuver failure.

6. Conclusions

The paper presented the steps followed to design a suitable trajectory for the LICIA CubeSat, to meet the stringent constraints imposed by the mission, and highlighting the challenges related to the employment of such systems in a deep-space environment.

In particular, the designed trajectory has been refined according to several mission requirements arising from science objectives, platform performances, operational requirements, and safety margins. The scientific target of the mission imposed a minimum resolution constraint for the imaging of both impact site and plume expansion (from DART impact), and of the side of the asteroid not visible from DART. Limitations arising from platform mainly involved the ADCS subsystem: pointing requirements constrained the flyby to a distance greater than 44 km, thus hindering an imaging at 1 m/px resolution, required for crater observation. Nevertheless, preliminary analyses of the expected crater dimensions on the sensor revealed low chances of visualization and characterization, leading to the downgrade of this mission objective in favor of ejecta plume and asteroid's surface characterization.

The limited propulsive capabilities did not represent an issue for the mission design. In fact, the operative necessity of a release 5 days before DART impact ensures a time window long enough to achieve the required separation from the asteroid with a low amount of fuel. Also, propulsion performances

demonstrated to withstand contingency scenarios, with delayed maneuvers and higher ΔVs.

The refined trajectory of the CubeSat is robust to all uncertainties related to the platform, DART, Didymos, and the ground tracking for orbit determination, and ensures limited variations in the trajectory performance.

The trajectory design of the CubeSat is in constant evolution, due to the frequent refinements in the platform and operations (for both LICIA and DART); however, the results presented in this paper show the rationale behind the development of such trajectory, with particular attention to the identification of the achievable close approach performance, which have been set as target values to be maintained, regardless of the possible future changes in the mission operations (e.g. number of maneuvers, release conditions, etc.).

The current efforts in mission design will allow LICIA spacecraft to be the first CubeSat to fly by an asteroid, setting the path for the future of low cost exploration missions around small bodies. Its contribution will provide crucial information about Near Earth Objects structure and composition, dramatically enhancing the scientific outcome of the DART mission.

7. Acknowledgements

This research was funded by the Italian Space Agency under the implementing agreement No. 2019-31-HH.0.

References

[1] M. Ashman, M. Barthélémy, M. Almeida, N. Altobelli, M.C. Sitjà, J.J.G. Beteta, B. Geiger, B. Grieger, D. Heather, R. Hoofs, et al. Rosetta

science operations in support of the philae mission. *Acta Astronautica*, 125:41–64, 2016.

[2] C. Lange, J. Biele, S. Ulamec, C. Krause, B. Cozzoni, O. Küchemann, S. Tardivel T., Ho, C. Grimm, J.T. Grundmann, et al. Mascot2–a small body lander to investigate the interior of 65803 didymos' moon in the frame of the aida/aim mission. *Acta Astronautica*, 149:25–34, 2018.

[3] Hannah Goldberg, Özgür Karatekin, Birgit Ritter, Alain Herique, Paolo Tortora, Claudiu Prioroc, Borja Garcia Gutierrez, Paolo Martino, Ian Carnelli, and Borja Garcia. The juventas cubesat in support of esa's hera mission to the asteroid didymos. In *Small Satellite Conference, Logan, Utah*, 2019.

[4] A.F. Cheng, J. Atchison, B. Kantsiper, A.S. Rivkin, A. Stickle, C. Reed, A. Galvez, I. Carnelli, P. Michel, and S. Ulamec. Asteroid impact and deflection assessment mission. *Acta Astronautica*, 115(Supplement C):262 – 269, 2015.

[5] Martin T Ozimek and Justin A Atchison. Nasa double asteroid redirection test (dart) low-thrust trajectory concept. In *27th AAS/AIAA Space Flight Mechanics Meeting, San Antonio, USA*, volume 221, 2017.

[6] A. Capannolo, V. Pesce, and M. Lavagna. Binary asteroid redirection: science opportunity for nanosats. In *69th International Astronautical Congress (IAC 2018)*, pages 1–13, 2018.

[7] R.A. Werner and D.J. Scheeres. Exterior gravitation of a polyhedron derived and compared with harmonic and mascon gravitation represen-

tations of asteroid 4769 castalia. *Celestial Mechanics and Dynamical Astronomy*, 65:313–344, 1997.

[8] W.D. MacMillan. *The theory of the potential*, chapter 35–36, pages 56–60. Dover, 1958.

[9] V. Szebehely. *Theory of Orbits: The Restricted Problem of Three Bodies*. Academic Press, New York and London, 1967.

[10] E. Dotto, V. Della Corte, M. Amoroso, I. Bertini, J.R. Brucato, A. Capannolo, G. Cremonese, B. Cotugno, V. Di Tana, I. Gai, et al. Liciacube - the light italian cubesat for imaging of asteroids in support of the nasa dart mission towards asteroid (65803) didymos. *Planetary and Space Science*, 2020.

[11] K.A. Holsapple and R.M. Schmidt. On the scaling of crater dimensions - 2. impact processes. *Journal of Geophysical Research*, 87(B3):1849–1870, 1982. Cited By :183.

[12] K.R. Housen and K.A. Holsapple. Ejecta from impact craters. *Icarus*, 211(1):856–875, 2011.

[13] J.E. Richardson, H.J. Melosh, C.M. Lisse, and B. Carcich. A ballistics analysis of the deep impact ejecta plume: Determining comet tempel 1's gravity, mass, and density. *Icarus*, 190(2):357–390, 2007.

[14] E. Buhl, F. Sommer, M.H. Poelchau, G. Dresen, and T. Kenkmann. Ejecta from experimental impact craters: Particle size distribution and fragmentation energy. *Icarus*, 237:131–142, 2014.

[15] H. Miyamoto, H. Yano, D.J. Scheeres, S. Abe, O. Barnouin-Jha, A.F. Cheng, H. Demura, R.W. Gaskell, N. Hirata, M. Ishiguro, T. Michikami, A.M. Nakamura, R. Nakamura, J. Saito, and S. Sasaki. Regolith migration and sorting on asteroid itokawa. *Science*, 316(5827):1011–1014, 2007.

[16] Y. Yu and P. Michel. Ejecta cloud from the aida space project kinetic impact on the secondary of a binary asteroid: Ii. fates and evolutionary dependencies. *Icarus*, 312:128–144, 2018.

[17] G. Zanotti. Hypervelocity impacts on planetary bodies: Modelling craters formation and ejecta plume evolution. Master's thesis, Politecnico di Milano, Dipartimento di Scienze e Tecnologie Aerospaziali, Milano, Italy, 2019.

[18] G. Zanotti, A. Capannolo, and M. Lavagna. Assessment on small bodies impacts and fragments plume dynamics modelling through sph with ls-dyna solver. In *EGU General Assembly 2019*, Vienna, Austria, 2019.

[19] G. Drolshagen. Impact effects from small size meteoroids and space debris. *Advances in space Research*, 41(7):1123–1131, 2008.

[20] J.A. Atchison, M. Abrahamson, M. Ozimek, B. Kantsiper, E.Y. Adams, A.F. Cheng, A.S. Rivkin, C. Reed, S. Bhaskaran, Z. Tarzi, et al. Double asteroid redirection test (dart) mission design and navigation for low energy escape. In *69th International Astronautical Congress*, 2018.